

Scaffolding Functions of Arrestin-2 Revealed by Crystal Structure and Mutagenesis^{†,‡}

Shawn K. Milano,[§] Helen C. Pace,[§] You-Me Kim,^{||} Charles Brenner,^{*,§} and Jeffrey L. Benovic^{*,||}

Structural Biology and Bioinformatics Program and Cell Biology and Signaling Program, Kimmel Cancer Center, Thomas Jefferson University, Philadelphia, Pennsylvania 19107

Received October 31, 2001; Revised Manuscript Received December 26, 2001

ABSTRACT: Arrestin binding to activated, phosphorylated G protein-coupled receptors (GPCRs) represents a critical step in regulation of light- and hormone-dependent signaling. Nonvisual arrestins, such as arrestin-2, interact with multiple proteins for the purpose of propagating and terminating signaling events. Using a combination of X-ray crystallography, molecular modeling, mutagenesis, and binding analysis, we reveal structural features of arrestin-2 that may enable simultaneous binding to phosphorylated receptor, SH3 domains, phosphoinositides, and β -adaptin. The structure of full-length arrestin-2 thus provides a uniquely oriented scaffold for assembly of multiple, diverse molecules involved in GPCR signal transduction.

Many transmembrane signaling systems consist of specific G protein-coupled receptors (GPCRs)¹ that transduce the binding of a diverse array of extracellular stimuli into intracellular signaling events (1). GPCRs modulate the activity of numerous effector molecules including adenylyl cyclases, PI 3-kinases, nonreceptor tyrosine kinases, small G proteins, phosphodiesterases, phospholipases, and ion channels. To ensure that extracellular stimuli are translated into intracellular signals of appropriate magnitude and specificity, these signaling cascades are tightly regulated. GPCRs are subject to three principal modes of regulation: desensitization, in which a receptor becomes refractory to continued stimuli; endocytosis, whereby receptors are removed from the cell surface; and downregulation, in which total cellular receptor levels are decreased (2, 3).

GPCR desensitization is primarily mediated by second messenger-dependent kinases, such as protein kinase A and protein kinase C, and by G protein-coupled receptor kinases (GRKs). GRKs specifically phosphorylate activated GPCRs, initiating recruitment of arrestins. Arrestins are divided into two major classes, visual and nonvisual, on the basis of localization. The nonvisual arrestins, arrestin-2 and arrestin-3

(also termed β -arrestin-1 and -2), are broadly distributed and function in multiple processes. While a role for arrestins in GPCR desensitization has been appreciated for many years (4, 5), recent insight has implicated nonvisual arrestins in regulation of GPCR trafficking (6, 7). Multiple interactions contribute to arrestin-mediated trafficking of GPCRs including a C-terminal insert region in nonvisual arrestins that binds the terminal domain of clathrin heavy chain (8, 9), a C-terminal region that interacts with the β -subunit of the heterotetrameric AP2 complex (β -adaptin) (10), and a basic region that binds phosphoinositides (11).

Recent studies also support a direct role for arrestins in GPCR signaling. Proline-rich region(s) in arrestin-2 have been shown to mediate binding to the SH3 domain in Src (12). The catalytic domain of Src may also contribute to arrestin binding (13). Additional evidence for arrestin interaction with Src family members was found in neutrophils, in which treatment with interleukin-8, which activates the chemokine receptor CXCR1, promotes interaction of arrestin-2 with tyrosine kinases Hck and c-Fgr (14). Recent findings also suggest a role for arrestins as MAP kinase scaffolds. Work from Bunnett and co-workers demonstrated formation of complexes that contain receptor (either PAR2 or neurokinin-1), arrestin-2, ERK1/2, and either Raf-1 or Src (15, 16). Similarly, Lefkowitz, Davis, and co-workers demonstrated that arrestin-3 binds JNK3 and ASK1, a JNK kinase kinase, suggesting a role for arrestin-3 as a MAP kinase scaffold (17). Thus, nonvisual arrestins may play a critical role in mediating GPCR activation of tyrosine kinase and MAP kinase pathways.

Initial structural insight on arrestins was provided by crystal structures of bovine visual arrestin (arrestin-1) reported by the groups of Granzin (18) and Sigler (19). These studies revealed that arrestin-1 is a molecule containing two domains made up of β -sheets joined by a set of buried salt bridges termed the polar core (19). Further, the structure was interpreted in light of mutagenic and biophysical studies to describe the basal form of arrestin, with binding to phos-

[†] This work was supported in part by National Institutes of Health Grant GM47417 (to J.L.B.). S.K.M. was supported by National Institutes of Health Training Grant T32-CA07403 while Y.-M.K. was supported by a fellowship from the American Heart Association. This work is based upon research conducted at the Cornell High Energy Synchrotron Source (CHESS), which is supported by the National Science Foundation under Award DMR 97 13424.

[‡] The atomic coordinates and structure factor file for arrestin-2 have been deposited in the Protein Data Bank with the accession code 1JSY.

* Correspondence and requests for materials should be addressed to J.L.B. or C.B. (e-mail: benovic@lac.jci.tju.edu or brenner@lada.jci.tju.edu).

[§] Structural Biology and Bioinformatics Program.

^{||} Cell Biology and Signaling Program.

¹ Abbreviations: GPCRs, G protein-coupled receptors; GRKs, G protein-coupled receptor kinases; PIP₂, phosphatidylinositol 4,5-bisphosphate; PMSF, phenylmethanesulfonyl fluoride; ADAP, GST- β -adaptin appendage domain; TD, GST-clathrin terminal domain; STD, standards; WT, wild type.

phorylated receptor proposed to disrupt the polar core and lead to an altered conformation (19, 20). Functioning in hormone-dependent GPCR regulation rather than light-dependent rhodopsin regulation, arrestin-2 has distinct molecular properties. Whereas arrestin-1 specifically recognizes phosphorylated rhodopsin, arrestin-2 binds a wide variety of phosphorylated GPCRs (2, 21). In addition, arrestin-2 binds phosphoinositides (11), SH3 domain-containing proteins (12, 14), clathrin (7), and β -adapin (22). Although the recent crystal structures of two C-terminally truncated forms of arrestin-2 provide insight into GPCR binding (23), the structural basis for many of arrestin's additional interactions remains largely unknown.

Here, we report the crystal structure of full-length arrestin-2. Unlike arrestin-1, which exists as a dimer in solution (24), arrestin-2 is monomeric. The refined structure at 2.9 Å resolution provides several important insights. It defines regions that may account for differences in receptor binding, locates phospholipid binding in a manner that orients the molecule toward the membrane, and identifies sites that could be utilized by SH3 domain-containing signaling partners. In addition, we provide a model for association of arrestin-2 and β -adapin that is supported by biochemical and molecular analysis. Each of these interactions appears to be nonoverlapping, enabling arrestin-2 to scaffold receptor, downstream kinases, and components of the endocytic machinery within a membrane microdomain.

MATERIALS AND METHODS

Expression and Purification of Arrestin-2. Recombinant arrestin-2 was expressed in BL21(DE3)-lysS bacterial cells using a bovine arrestin-2 cDNA cloned into the expression vector pTrcHisB (without the His tag). Cells were grown in terrific broth containing 0.1 mg/mL ampicillin and 0.04 mM IPTG for ~18 h at 30 °C, harvested by centrifugation, and lysed by freeze-thaw and polytron disruption in 20 mM Tris-HCl, pH 7.5, 10 mM EDTA, 2 mM dithiothreitol, 1 mM phenylmethanesulfonyl fluoride (PMSF), and 0.2 mg/mL benzamidine. The lysate was centrifuged (13000 rpm \times 30 min, GSA rotor), and the supernatant protein was then precipitated with $(\text{NH}_4)_2\text{SO}_4$ (36 g/100 mL of supernatant). The sample was centrifuged (13000 rpm \times 30 min, GSA rotor), and the pellet was dissolved in column buffer A (10 mM Tris-HCl, pH 7.5, 2 mM EDTA, 0.5 mM PMSF) and clarified by centrifugation (19000 rpm \times 20 min, SS34 rotor). The supernatant was dialyzed overnight against column buffer A containing 100 mM NaCl. The sample was then loaded on a heparin-Sepharose column and eluted with a 150–700 mM linear NaCl gradient in column buffer A. Peak fractions were pooled, diluted 8-fold with column buffer B (10 mM Tris-HCl, pH 7.5, 2 mM EDTA, 0.1 mg/mL benzamidine), loaded on a Q-Sepharose high-performance column, and eluted with a 50–250 mM linear NaCl gradient in column buffer B. Peak fractions were pooled, diluted 3-fold with column buffer C (10 mM HEPES, pH 7.2, 1 mM EDTA), loaded on an SP-Sepharose high-performance column, and eluted with a 40–250 mM linear NaCl gradient in column buffer C. Peak fractions were pooled, concentrated, frozen in liquid nitrogen, and stored at –80 °C until needed. Protein purity was >99%, based on SDS-PAGE and Coomassie blue staining, and typical yields were 5–10 mg of purified arrestin-2/L of culture.

Table 1: Crystallographic Data and Refinement Statistics

data collection	
space group	$P3_221$
unit cell (Å)	$a = b = 78.95, c = 158.92$
resolution (Å)	19–2.9
wavelength (Å)	0.948
mosaicity (deg)	0.401
unique reflections	13476
redundancy ^a	19.1
completeness (%)	99.9 (99.8) ^e
I/σ	11.9
R_{sym} (%) ^b	7.4 (31.8) ^e
refinement	
resolution (Å)	19–2.9
work reflections	11822
test reflections	1314
non-hydrogen protein atoms	2829
water molecules	76
R_{work} (%) ^c	22.98
R_{free} (%) ^d	23.85
average B -factor (Å ²)	57.8
RMSD from ideal values	
bond length (Å)	0.01
bond angle (deg)	1.58

^a Redundancy = total number of observations/unique reflections. ^b $R_{\text{sym}} = \sum |I - \langle I \rangle| / \sum \langle I \rangle$ in which I is a measured intensity and $\langle I \rangle$ is the average intensity from multiple measurements of symmetry-related reflections. ^c $R_{\text{work}} = \sum |F_o - F_c| / \sum F_o$. ^d R_{free} was calculated as for R_{work} using test reflections excluded from atomic refinement. ^e Data in parentheses refer to highest resolution bin.

Crystallization and Data Collection. Crystals were grown by hanging drop vapor diffusion. Drops consisted of 2 μL of protein solution (9 mg/mL in 10 mM HEPES, pH 7.2, 1 mM EDTA, 125 mM NaCl) and 0.5 μL of 40% polypropylene glycol 400 plus 2 μL of 150 mM magnesium formate and were equilibrated against 1 mL of 150 mM magnesium formate for 10 days. Crystals of dimensions 0.2 mm \times 0.1 mm \times 0.1 mm were transferred to 200 mM magnesium formate and 25% glycerol and flash-cooled in liquid nitrogen. Diffraction data were collected at the Cornell High Energy Synchrotron Source beamline F-1 at a crystal to detector distance of 220 mm with 1.5° oscillations.

Structure Determination and Refinement. Data were indexed and scaled using the HKL package (25). Crystals possessed the symmetry of space group $P3_121$ or $P3_221$ and contained a monomer in the asymmetric unit with 59% solvent. The structure was solved by molecular replacement using the program AMoRe (26). The arrestin-1 structure (19) was used as the search model with nonconserved residues changed to alanine and with arrestin-2 X-ray data truncated from 15 to 4.0 Å. The translation function in space group $P3_221$ produced a uniquely superior solution, with rigid body refinement yielding an R -factor of 45.7%. Refinement and building were carried out using the programs CNS (27) and O (28), respectively. Using data from 19 to 3.0 Å and a composite-omit map (27), much of the unaccounted density was traced, side chains were replaced, and loops that differed from arrestin-1 were rebuilt. After manual rebuilding, simulated annealing, and grouped B -factor refinement with a 1.5σ cutoff, the final atomic model was refined to 2.9 Å with $R_{\text{work}} = 22.98\%$ and $R_{\text{free}} = 23.85\%$. The model of arrestin-2 contains 358 amino acids and 76 water molecules. As shown in Table 1, the stereochemical parameters for the model calculated with PROCHECK (29) are reasonable and not indicative of excessive geometric restraint.

Analysis of Arrestin Interaction with β -Adaptin and Clathrin. A GST- β -adaptin appendage (residues 700–937) construct was provided by Dr. Harvey McMahon while a GST-clathrin terminal domain (residues 1–579) construct was supplied by Dr. James Keen. The proteins were expressed and purified on glutathione-agarose as described previously (8, 30). Purified arrestin-1 was prepared as described previously (7). Arrestin-2 mutations were generated by PCR and confirmed by DNA sequencing. Wild-type and mutant arrestins were expressed in COS-1 cells by transient transfection as described previously (31). Arrestin extracts were prepared by lysing the cells by freeze-thaw and polytron disruption in 20 mM HEPES, pH 7.2, 0.1 M NaCl, 0.02% Triton X-100, 10 mM EDTA, 0.5 mM PMSF, 0.02 mg/mL leupeptin, and 0.2 mg/mL benzamidine. The extracts were centrifuged (19000 rpm \times 20 min, SS34 rotor) and the supernatants aliquoted, frozen, and stored at -80°C until needed (extracts contained $\sim 2\ \mu\text{g}$ of arrestin/mL).

Purified arrestins (200–400 ng) or arrestin-containing lysates ($\sim 20\ \text{ng}$ of arrestin) were incubated with $5\ \mu\text{L}$ of glutathione-agarose beads (containing $\sim 10\ \mu\text{g}$ of bound GST or GST fusion protein) in binding buffer (20 mM HEPES, pH 7.2, 120 mM potassium acetate, 0.1 mM dithiothreitol, 0.1% Triton X-100) for 1 h at 4°C (in a total volume of $100\ \mu\text{L}$). The beads were then pelleted in a microcentrifuge (1000 rpm \times 5 min) and washed two to three times with $0.5\ \text{mL}$ of binding buffer, and bound arrestin was eluted by boiling the beads in SDS sample buffer for 10 min. The samples were electrophoresed on a 10% polyacrylamide gel, transferred to nitrocellulose, and then detected by immunoblotting using mouse monoclonal (F4C1) or purified rabbit polyclonal (178) anti-arrestin antibodies, HRP-labeled goat anti-mouse or anti-rabbit secondary antibodies and chemiluminescence using SuperSignal (Pierce).

Docking Analysis. All docking was performed using the manual matching option in Dock version 4.0 (32). Three basic residues in arrestin-3 are known to be required for phosphoinositide binding (11), so the search region was set up to contain the analogous side chains in arrestin-2. One residue, Lys-232, with weak side chain electron density for a nonstandard conformation was replaced with a standard Lys rotamer from the O library (28). Arrestin-2 has high affinity for several different inositol phosphates and phosphoinositides in vitro, although phosphatidylinositol 4,5-bisphosphate (PIP₂) and phosphatidylinositol 3,4,5-trisphosphate (PIP₃) will likely serve as primary in vivo ligands (11). Rigid docking of the PIP₂ analogue, L- α -glycerophospho-D-myoinositol 4,5-bisphosphate (IBS from PDB ID no. 117E) (33), was performed. Several top solutions were inspected and the one shown in Figure 3C was selected on the basis of its implications for specific recognition. The arrestin-2 model with β -adaptin was obtained by allowing an eight amino acid peptide segment (residues 390–397) of arrestin-2 to dock flexibly in the β -adaptin binding pocket. The best solution is shown in Figure 4C.

RESULTS AND DISCUSSION

Arrestin-2 Structure Determination. The crystal structure of full-length arrestin-2 (1–418) was solved by molecular replacement using arrestin-1 (19) as the search model and refined to $2.9\ \text{\AA}$ (Figure 1). The trigonal crystals contained an arrestin-2 monomer in the asymmetric unit with dimen-

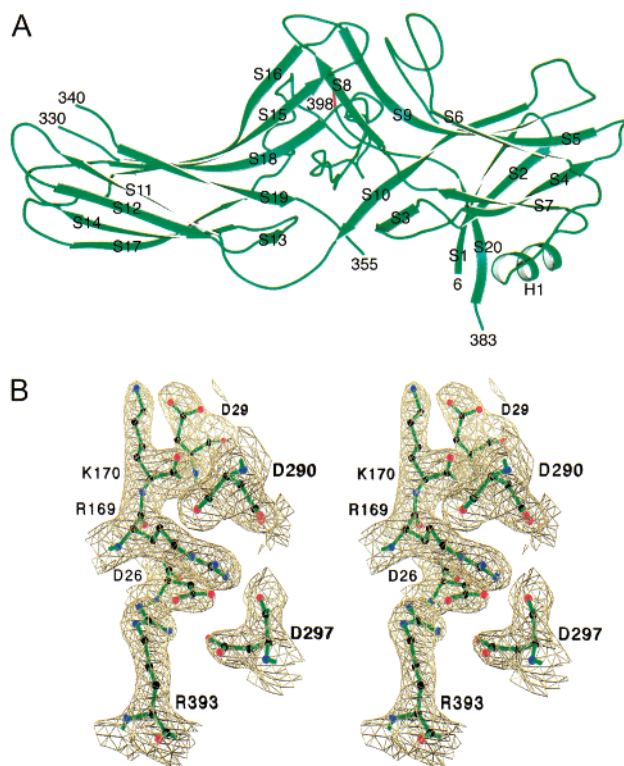


FIGURE 1: Arrestin-2 secondary structure and polar core. (A) Standard view of arrestin-2 showing the secondary structure elements (strands numbered S1 to S20) and a single helix, H1. The residues at the beginning and ending gap regions are numbered; the C-terminal stretch from 398 to 399 is shown in red because it is partially obscured in view. (B) $2F_o - F_c$ electron density map contoured at 1.2σ surrounding the distinctive polar core. The map illustrates unambiguous electron density for these highly conserved residues. Panel A was produced with Molscript (40), Povscript (<http://cerebus.biochem.med.umich.edu/~peisach/povscript/>), and POV-Ray (<http://www.povray.org>). Panel B was produced with Swiss-Pdb Viewer (41) and POV-Ray.

sions of approximately $95 \times 50 \times 45\ \text{\AA}$. The current model includes residues 6 through 330, 340 through 355, and 383 through 399. Absence of electron density for 5 N-terminal, 19 C-terminal, and 36 internal residues has prevented these sections of the polypeptide from being built. The refined model of full-length arrestin-2 is strikingly similar to the recent structures of two C-terminally truncated forms of arrestin-2, 1–393 and 1–382 (23). The clathrin binding site and most of the residues (334–340) missing in a splice variant of arrestin-2 are disordered in all crystal forms. Minor structural differences between the arrestin-2 forms occur mostly in solvent-exposed loops. Unlike full-length and the 1–393 truncated proteins, the 1–382 mutant is constitutively active and able to bind GPCRs in a phosphorylation-independent manner (34). Nonetheless, the crystal structure of the 1–382 truncated arrestin-2 did not reveal a physical basis for altered biological function (23). Here we examine the structure of arrestin-2 to identify features responsible for protein–protein and protein–phosphoinositide interactions.

Like arrestin-1, arrestin-2 consists of 20 β -strands and a single α -helix arranged into what has been termed the N-domain, containing strands S1 through S10, helix H1 and strand S20, and the C-domain, containing strands S11 through S19 (19). In arrestin-2, the linker between the two domains is formed by residues 174 through 181. The polar

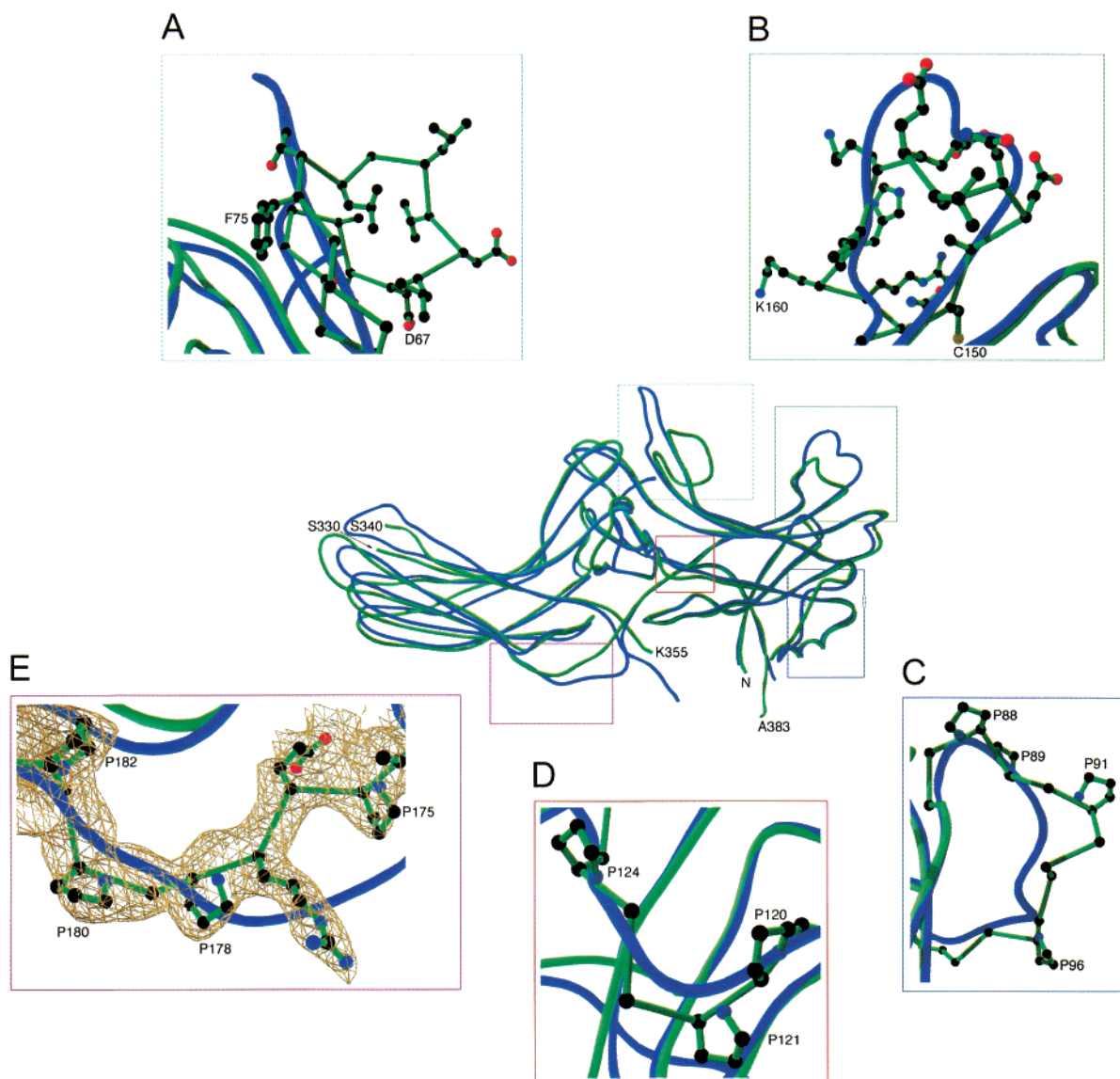


FIGURE 2: Differences between arrestin-2 and arrestin-1 structures. The center of the figure shows the least squares superposition of arrestin-2 in green and arrestin-1 (α -conformer) in blue. The RMSD for the two molecules using 353 C α atoms is 3.66 Å. Regions of notable dissimilarity between the proteins are outlined in boxes, which are enlarged for greater detail. (A) Connecting loop S5–S6 in arrestin-2 is compared with the respective loop in arrestin-1. The enclosed flap of arrestin-2 can clearly be seen when overlaid with the tight β -turn in arrestin-1. The side chains of arrestin-2 are depicted for emphasis. (B) Close-up view showing the connecting loop S9–S10 in arrestin-2 against the corresponding region in arrestin-1. Arrestin-2 appears to have an enclosed, coil structure whereas arrestin-1 contains a short α -helix. The side chains of arrestin-2 are displayed for clarity. (C) Proline-rich region 1: potential SH3 binding region, P⁸⁸xxP⁹¹. (D) Proline-rich region 2: a second apparent SH3 binding region, P¹²¹xxP¹²⁴. (E) Proline-rich region 3: a putative third SH3 binding region, P¹⁷⁵xxP¹⁷⁸, containing the same classical PxxP motif as in regions 1 and 2. Difference ($F_o - F_c$) electron density contoured at 2.0σ is shown for this polyproline region. The figures were made with Swiss-Pdb Viewer (41) and POV-Ray.

core of buried salt bridges attaching the two domains in arrestin-1 is fully conserved in arrestin-2 and includes Asp-26, Arg-169, Lys-170, Asp-290, Asp-297, and Arg-393 (Figure 1B). It has been suggested that disruption of the polar core by phosphorylated receptor results in a conformational change in arrestin that enhances receptor binding (19, 20). Although the receptor-bound conformation of arrestin is not known, arrestin-1 binding to phosphorylated receptor results in a structural rearrangement (35) that exposes its C-terminal region (36). Release of the C-terminal region appears to disrupt the basal state of arrestin by breaking hydrophobic interactions within the N-domain including α -helix H1 (37).

Significant structural differences between arrestin-2 and arrestin-1 are shown in Figure 2. The central part of the figure

shows a least squares superposition of arrestin-2 (green) with the α -conformer of arrestin-1 (blue). While the root mean square difference calculated for all 353 alignable C α residues is 3.66 Å, we focus on five areas of structural divergence, two that may participate in receptor binding (Figure 2, panels A and B) and three that are apparent SH3 binding domains (Figure 2, panels C–E).

Arrestin-2 Has a Distinct Saddle for Binding Phosphorylated Receptor. It is important to note that arrestin-1 is highly specific for binding activated phosphorylated rhodopsin while arrestin-2 binds most phosphorylated GPCRs (2, 21). The molecular basis for these preferences was until recently largely unknown. Segment-swapping experiments between arrestin-1 and arrestin-2 have revealed residues 50–90 of

arrestin-1 important for receptor binding and specificity (23). In fact, a single amino acid change in arrestin-1, V90S, is sufficient to enable arrestin-1 to bind activated m2 muscarinic cholinergic receptor with an affinity similar to that of arrestin-2 (23). The equivalent region in arrestin-2 (residues 46–86) is found in what we term the “saddle” region, the primary binding site of phosphorylated GPCR. This region consists of strands S5 (residues 52–59), S6 (residues 80–85), S9 (residues 138–149), and S10 (residues 164–174) and the S5–S6 (residues 60–79) and S9–S10 (residues 150–163) connecting loops. There are two main structural differences between the saddle regions in arrestin-1 and arrestin-2. First, as shown in Figure 2, panels A and B, the two connecting loops in arrestin-2 are in substantially more closed conformations relative to the respective loops in the α -conformer of arrestin-1 (19). Second, in the arrestin-1 α -conformation, the region that forms the S5–S6 loop in arrestin-2 is engaged in a tight β -turn. Similarly, in the arrestin-1 β -conformation (19), the S9–S10 region is in a tight β -turn (not shown). If the S5–S6 and S9–S10 loops are important for phosphorylated GPCR binding, then substantial activation energy might be required to release residues forming intramolecular β interactions in arrestin-1. Thus, tight S5–S6 and S9–S10 turns in arrestin-1 may result in its higher specificity for rhodopsin sequences. Less rigid and more enclosed S5–S6 and S9–S10 loops seen in arrestin-2 may be conformations that contribute to GPCR binding promiscuity.

SH3 Domain Recognition Motifs in Arrestin-2. Nonvisual arrestins function as scaffolding proteins to regulate GPCR-mediated activation of nonreceptor tyrosine kinases and MAP kinases. The best characterized of these interactions is that between arrestin-2 and c-Src (12). Arrestin-2 appears to interact with c-Src at multiple sites including its SH3 domain (via arrestin-2's proline-rich regions) (12) and its catalytic SH1 domain (13). Moreover, the phosphorylation state of Ser-412, an ERK1/2 phosphorylation site in arrestin-2 (38), has been implicated in mediating receptor-dependent association of arrestin-2 and c-Src (12). Three proline-rich motifs in arrestin-2 could potentially contribute to SH3 domain interaction: P⁸⁸xxP⁹¹, P¹²¹xxP¹²⁴, and P¹⁷⁵xxP¹⁷⁸ (where x is any amino acid). Importantly, these PxxP signature sequences are solvent exposed and easily accessible for protein–protein interactions. As shown in Figure 2, panels C–E, these proline-rich motifs are the three most distinctive features of the under side of arrestin-2 vis à vis arrestin-1. Though the crystal structure does not provide insight into which of these regions directly contribute to SH3 domain interaction, a P91A/P121E mutant arrestin-2 has significantly reduced binding to Src (13) and Hck (14). Notably, the putative SH3-docking regions of arrestin-2 each appear to be independent of and noncompetitive with the receptor binding and phosphoinositide binding regions of arrestin-2.

Phosphoinositide Binding by Arrestin-2. Previous studies have identified an important role for nonvisual arrestin interaction with phosphoinositides (11), clathrin (7), and β -adaptin (10) in GPCR trafficking. Three basic residues in arrestin-3 (Lys-233, Arg-237, and Lys-251) have been implicated in high-affinity binding to phosphoinositides (11). As shown in Figure 3A, these residues are located on the face of arrestin-2 containing the phosphorylated receptor binding saddle, such that receptor could sit in the saddle

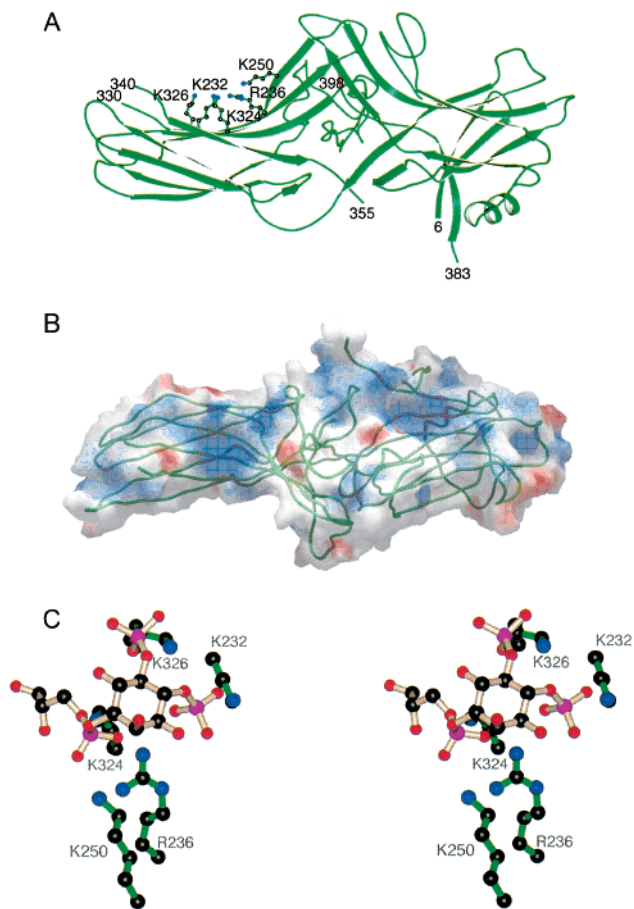


FIGURE 3: Modeling of arrestin-2 phosphoinositide binding site. (A) Standard view as in Figure 1A with five basic residues in the phosphoinositide binding site (labeled) shown in ball-and-stick representation. (B) Basic face of the electrostatic surface (top of view in panel A is rotated 90° toward viewer). The surface has a transparency factor of 0.5 to allow the backbone worm (in green) to be seen beneath the surface. The electrostatic potential was calculated in GRASP (42) using a full charge set with inner and outer dielectrics of 2.0 and 80.0, respectively. Ionic strength was set to 150 mM, and cutoff values for negative and positive potential were set to -10 and $+10$ kt. (C) Stereoview of a closeup of the C-terminal domain (as in panel A but rotated 90° toward the viewer) with docked L- α -glycerophospho-D-myoinositol 4,5-bisphosphate and interacting side chains (labeled) in ball-and-stick representation.

while these basic residues recognize a phosphoinositide headgroup. In Figure 3B, the model was rotated 90° to allow viewing of the electrostatic surface potential of the membrane-proximal face of arrestin-2. The membrane-proximal surface of each domain contains a highly electropositive surface. To provide a more specific prediction of how arrestin-2 might bind a phosphoinositide headgroup, we investigated how the PIP₂ analogue L- α -glycerophospho-D-myoinositol 4,5-bisphosphate might interact with this surface. As shown in Figure 3C, it appears that the C-domain basic patch forms a specific binding site for a single phosphoinositide headgroup and that phosphate oxygens at positions 1 and 4 of the PIP₂ analogue can form strong hydrogen bonds with Lys-250 and Lys-232 side chain ζ -nitrogens, respectively. Arg-236 is in a position to bridge oxygens from phosphates 1 and 4. Arg-236 and Lys-232 are both located on β -strand S15. Two additional residues (Lys-324 and Lys-326) are located in the immediately adjacent β -strand S18 and appear to be in a position to contribute additional specificity. Our model places

the ζ -nitrogen of Lys-324 near the glycerophosphate oxygen and that of Lys-326 interacting with one of the P5 oxygen atoms. This biochemically defined and structurally modeled phosphoinositide binding site is critical for GPCR endocytosis (11).

Arrestin-2 Interaction with β -Adaptin. Although previous studies suggested that binding of arrestin to β -adaptin is critical for GPCR internalization, these studies did not address whether this is via direct interaction of these proteins (10). To test whether arrestin-2 directly binds to β -adaptin, we assayed binding of arrestin to glutathione *S*-transferase- β -adaptin fusion proteins. As shown in Figure 4A (right panel), arrestin-2 binds to a similar extent with the appendage domain of β -adaptin and the terminal domain of clathrin. The specificity of the interaction is revealed by the demonstration that purified arrestin-2, but not arrestin-1, can bind β -adaptin (Figure 4A, left panel). These results reveal that arrestin-2 binds directly to the β -adaptin appendage, a domain implicated in interactions with multiple proteins including clathrin, AP180, eps15, and epsin (30).

Previous studies suggested that two C-terminal arginine residues in arrestin-3 are critical for β -adaptin binding (10). The corresponding residues in arrestin-2 are Arg-393 and Arg-395. To further probe contributions of arrestin residues to adaptin binding, we constructed and expressed several mutant arrestin-2 proteins including E389R, D390R, F391A, R393E, Q394A, R395E, and L396A alleles. Binding analysis suggested a critical role for Phe-391, Arg-395, and Leu-396 in β -adaptin binding (Figure 4B, upper panel). Mutation of Arg-393 had no effect on adaptin binding, but examination of the crystal structure reveals that this residue contributes to a conserved, buried salt bridge with Asp-26 in the polar core and thus is unlikely to mediate binding to other proteins in the basal state. Although the R395E mutation was completely disrupted in adaptin binding, this mutation also had reduced binding to clathrin (Figure 4B, lower panel). This is in contrast to all of the other arrestin-2 mutants that were unaffected in clathrin binding (Figure 4B, lower panel). Because Arg-395 does not appear to be involved in any intramolecular interactions (Figure 1) and thus is unlikely to cause a global disruption of arrestin structure when mutated, it seems likely that Arg-395 is directly involved in β -adaptin and clathrin interaction.

Given the important role of Phe-391, Arg-395, and Leu-396 in β -adaptin binding, we attempted to identify a unique location and orientation of the interaction between arrestin-2 and the appendage domain of β -adaptin (Figure 4C). This analysis predicts involvement of multiple β -adaptin residues in arrestin binding including Trp-841 and Tyr-888 interaction with Phe-391 and Glu-849 and Glu-902 interaction with Arg-395. Additional interactions predicted by our model include Arg-904 with Asp-390 and Glu-882 with Arg-393 although we speculate that these residues would only be accessible in the activated conformation of arrestin-2. Indeed, initial studies reveal that an activated form of arrestin-2 (an R169E mutation) binds β -adaptin much better than does wild-type arrestin-2 (data not shown). We were unable to determine the basis for Leu-396 specificity from our docking analysis. Overall, these studies reveal a significant ionic and hydrophobic interface between arrestin-2 and β -adaptin that mediates the specific interaction of these proteins. Although the location of β -adaptin binding is compatible with simul-

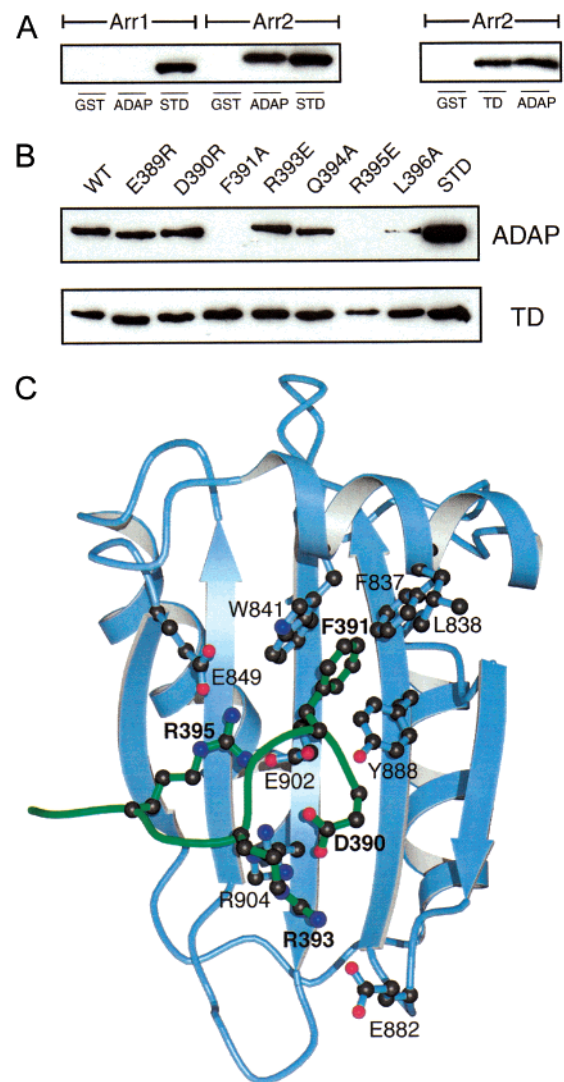


FIGURE 4: Binding analysis and modeling of arrestin-2 interaction with the AP2 β -appendage domain. (A) Left panel: Purified arrestin-1 or arrestin-2 (400 ng each) was incubated with $\sim 10 \mu\text{g}$ of GST or GST- β -adaptin appendage domain (ADAP), and bound arrestin was detected by immunoblotting as described in Materials and Methods. The standards (STD) represent 15% of the input. Right panel: Expressed arrestin-2 ($\sim 20 \text{ ng}$) was incubated with $\sim 10 \mu\text{g}$ of GST, GST-clathrin terminal domain (TD), or GST- β -adaptin appendage domain (ADAP), and bound arrestin was detected by immunoblotting as described in Materials and Methods. (B) Expressed wild-type (WT) or mutant arrestin-2 ($\sim 20 \text{ ng}$) was incubated with $\sim 10 \mu\text{g}$ of GST- β -adaptin appendage domain (ADAP) or GST-clathrin terminal domain (TD), and bound arrestin was detected by immunoblotting as described in Materials and Methods. The standards (STD) represent 40% of the input. All experiments in (A) and (B) were repeated at least three times. (C) Top view of the β -adaptin appendage domain of AP2 (30) in blue and arrestin-2 residues 390–397 in green. Side chains that interact are shown in ball-and-stick representation and are labeled in standard (β -adaptin) or bold (arrestin) font.

taneous binding of phosphorylated GPCR, phosphoinositide and SH3-containing proteins; β -adaptin and clathrin might compete for an overlapping site at the C-terminus of nonvisual arrestins. However, there is no evidence for such competition from studies examining arrestin-3 binding to purified clathrin cages and clathrin-coated vesicles *in vitro* or arrestin-2 association with clathrin-coated pits in cells (7).

Previous studies revealed that the primary clathrin binding site localized to a $L\phi X\phi E$ motif (in which ϕ is a bulky aliphatic residue) within an insert region in nonvisual arrestins (8). This motif is within an unstructured region of arrestin-2 (residues 356–382) found between β -strands S19 and S20 (Figure 1A), a region that was also unstructured in arrestin-1 and in truncated arrestin-2 (19, 23). Although these results provide no structural insight into arrestin/clathrin interaction, they suggest that this region of arrestin is disordered in the basal state and may require arrestin interaction with either receptor or clathrin to create a specific surface for clathrin binding. Indeed, a short peptide from this region of arrestin-3 has a defined structure when associated with clathrin (39).

Full-Length Arrestin-2 Is a Monomer in the Crystal and in Solution. A noncrystallographic interaction in arrestin-1 crystals that buried a 1041 Å² interface per monomer was interpreted as a head to tail dimer (24). The head to tail dimer, which extends two β -sheets in arrestin-1, is present as crystallographic symmetry in arrestin-2. The fact that arrestin-1 and arrestin-2 crystallize in a similar manner does not validate or invalidate the interaction. Because this set of contacts buries only 589 Å² per monomer in arrestin-2 and appears to interfere with its receptor and phosphoinositide binding ability, we interpret them merely as crystallization contacts and do not claim that the crystallographic dimer is biologically important.

To further analyze the oligomerization state of arrestin-2, purified arrestin-2 was subjected to analytical ultracentrifugation at concentrations of 10.6, 21.2, and 42.4 μ M. Material sedimented almost exclusively as a monomer with traces of material the size of a dimer. Fitting the data to a monomer–dimer equilibrium resulted in a calculated dissociation constant of 260 μ M (data not shown). Similar experiments with arrestin-1 allowed observation of apparent monomers, dimers, and larger species with a calculated dissociation constant of 34 μ M for dimers and a higher dissociation constant for larger species (24). As arrestin-1 (the second most abundant protein in rod outer segments) has an estimated in vivo concentration of 50–167 μ M, the postulated head to tail heterodimeric structure of arrestin-1 has been argued to be the favored dimeric unit (24). Because arrestin-2 has an \sim 8-fold higher dissociation constant for monomer–dimer equilibrium coupled with a lower cytosolic concentration, it is reasonable to assume that arrestin-2 is a monomer. Nevertheless, receptor clustering, localization in clathrin-coated pits, or other biological phenomena might create high local concentrations of arrestin-2 that could allow formation of complexes. Indeed, a truncated form of arrestin-2 (residues 1–382) lacking the C-tail was purified and reported to exist in solution as a 4 to 1 mixture of monomers to dimers, suggesting that release of the C-tail which occurs during receptor binding might promote dimer formation (23).

CONCLUSIONS

Substantial evidence indicates that arrestins require conformational changes to bind phosphorylated receptors, and the promiscuity of arrestin-2 in binding a variety of phosphorylated GPCRs has been a major unsolved problem. Here we show that arrestin-2 is a monomer with structurally unique S5–S6 and S9–S10 loops in its receptor binding saddle.

We hypothesize that this creates a promiscuous surface for receptor vis à vis that found in arrestin-1. Whereas many receptor domains may fit into the arrestin-2 saddle, arrestin-1 may depend on specific exchange of S5–S6 or S9–10 hydrogen bonds with rhodopsin sequences. Nonvisual arrestins are also unique in possessing binding sites for phosphoinositides, SH3-containing signaling proteins, and components of the endocytic machinery. Arrestin-2 appears to function as a scaffold oriented with its upper side bound to a phospholipid headgroup and phosphorylated receptor and its under side bound to SH3 proteins and to β -adaptin and/or clathrin. Thus, while arrestin-2 itself produces no second messenger, it organizes the basis for positive, negative, and restorative responses to hormone activation of GPCRs.

ACKNOWLEDGMENT

We thank Dr. James Lear for performing the analytical ultracentrifugation, Dr. Harvey McMahon for the GST–adaptin construct, Dr. James Keen for GST–clathrin, Dr. Vsevolod Gurevich for the arrestin-2 bacterial expression construct, Dr. Larry Donoso for the arrestin monoclonal antibody, and Drs. Raymond Penn and James Keen for constructive comments. We also thank William McCormick and RoseAnn Straquattonio for technical assistance.

REFERENCES

- Marinissen, M. J., and Gutkind, J. S. (2001) *Trends Pharmacol. Sci.* 22, 368–376.
- Krupnick, J. G., and Benovic, J. L. (1998) *Annu. Rev. Pharmacol. Toxicol.* 38, 289–319.
- Ferguson, S. S. G. (2001) *Pharmacol. Rev.* 53, 1–24.
- Wilden, U., Hall, S. W., and Kuhn, H. (1986) *Proc. Natl. Acad. Sci. U.S.A.* 83, 1174–1178.
- Lohse, M. J., Benovic, J. L., Caron, M. G., and Lefkowitz, R. J. (1990) *Science* 248, 1547–1550.
- Ferguson, S. S. G., Downey, W. E., III, Colapietro, A.-M., Barak, L. S., Menard, L., and Caron, M. G. (1996) *Science* 271, 363–365.
- Goodman, O. B., Jr., Krupnick, J. G., Santini, F., Gurevich, V. V., Penn, R. B., Gagnon, A. W., et al. (1996) *Nature* 383, 447–450.
- Krupnick, J. G., Goodman, O. B., Jr., Keen, J. H., and Benovic, J. L. (1997) *J. Biol. Chem.* 272, 15011–15016.
- Goodman, O. B., Jr., Krupnick, J. G., Gurevich, V. V., Benovic, J. L., and Keen, J. H. (1997) *J. Biol. Chem.* 272, 15017–15022.
- Laporte, S. A., Oakley, R. H., Holt, J. A., Barak, L. S., and Caron, M. G. (2000) *J. Biol. Chem.* 275, 23120–23126.
- Gaidarov, I., Krupnick, J. G., Falck, J. R., Benovic, J. L., and Keen, J. H. (1999) *EMBO J.* 18, 871–881.
- Luttrell, L. M., Ferguson, S. S., Daaka, Y., Miller, W. E., Maudsley, S., Della Rocca, G. J., et al. (1999) *Science* 283, 655–661.
- Miller, W. E., Maudsley, S., Ahn, S., Khan, K. D., Luttrell, L. M., and Lefkowitz, R. J. (2000) *J. Biol. Chem.* 275, 11312–11319.
- Barlic, J., Andrews, J. D., Kelvin, A. A., Bosinger, S. E., Dobransky, T., Feldman, R. D., Ferguson, S. S. G., and Kelvin, D. J. (2000) *Nat. Immunol.* 1, 227–233.
- DeFea, K. A., Zalevsky, J., Thoma, M. S., Dery, O., Mullins, R. D., and Bunnnett, N. W. (2000) *J. Cell Biol.* 148, 1267–1281.
- DeFea, K. A., Vaughn, Z. D., O'Bryan, E. M., Nishijima, D., Dery, O., and Bunnnett, N. W. (2000) *Proc. Natl. Acad. Sci. U.S.A.* 97, 11086–11091.

17. McDonald, P. H., Chow, C. W., Miller, W. E., Laporte, S. A., Field, M. E., Lin, F. T., et al. (2000) *Science* 290, 1574–1577.
18. Granzin, J., Wilden, U., Choe, H. W., Labahn, J., Krafft, B., and Büldt, G. (1998) *Nature* 391, 918–921.
19. Hirsch, J. A., Schubert, C., Gurevich, V. V., and Sigler, P. B. (1999) *Cell* 97, 257–269.
20. Vishnivetskiy, S. A., Paz, C. L., Schubert, C., Hirsch, J. A., Sigler, P. B., and Gurevich, V. V. (1999) *J. Biol. Chem.* 274, 11451–11454.
21. Gurevich, V. V., Dion, S. B., Onorato, J. J., Ptasienski, J., Kim, C. M., Sterne-Marr, R., et al. (1995) *J. Biol. Chem.* 270, 720–731.
22. Laporte, S. A., Oakley, R. H., Zhang, J., Holt, J. A., Ferguson, S. S. G., Caron, M. G., and Barak, L. S. (1999) *Proc. Natl. Acad. Sci. U.S.A.* 96, 3712–3717.
23. Han, M., Gurevich, V. V., Vishnivetskiy, S. A., Sigler, P. B., and Schubert, C. (2001) *Structure* 9, 869–880.
24. Schubert, C., Hirsch, J. A., Gurevich, V. V., Engelman, D. M., Sigler, P. B., and Fleming, K. G. (1999) *J. Biol. Chem.* 274, 21186–21190.
25. Otwinowski, Z., and Minor, W. (1997) *Methods Enzymol.* 276, 307–326.
26. Navaza, J. (1994) *Acta Crystallogr., Sect. D* 50, 157–163.
27. Brunger, A. T., Adams, P. D., Clore, G. M., DeLano, W. L., Gros, P., Grosse-Kunstleve, R. W., et al. (1998) *Acta Crystallogr., Sect. D* 54, 905–921.
28. Jones, T. A., Zou, J.-Y., Cowan, W. W., and Kjeldgaard, M. (1991) *Acta Crystallogr., Sect. A* 47, 110–119.
29. Laskowski, R. A., MacArthur, M. W., Moss, D. S., and Thornton, J. M. (1993) *J. Appl. Crystallogr.* 26, 283–291.
30. Owen, D. J., Vallis, Y., Pearse, B. M. F., McMahon, H. T., and Evans, P. R. (2000) *EMBO J.* 19, 4216–4227.
31. Orsini, M. J., and Benovic, J. L. (1998) *J. Biol. Chem.* 273, 34616–34622.
32. Ewing, T. J. A., and Kuntz, I. D. (1997) *J. Comput. Chem.* 18, 1175–1189.
33. Santagata, S., Boggon, T. J., Baird, C. L., Gomez, C. A., Zhao, J., Shan, W. S., et al. (2001) *Science* 292, 2041–2050.
34. Kovoov, A., Celver, J., Abdryashitov, R. I., Chavkin, C., and Gurevich, V. V. (1999) *J. Biol. Chem.* 274, 6831–6834.
35. Schleicher, A., Kuhn, H., and Hofmann, K. P. (1989) *Biochemistry* 28, 1770–1775.
36. Ohguro, H., Palczewski, K., Walsh, K. A., and Johnson, R. S. (1994) *Protein Sci.* 3, 2428–2434.
37. Vishnivetskiy, S. A., Schubert, C., Climaco, G. C., Gurevich, Y. V., Velez, M.-G., and Gurevich, V. V. (2000) *J. Biol. Chem.* 275, 41049–41057.
38. Lin, F. T., Krueger, K. M., Kendall, H. E., Daaka, Y., Fredericks, Z. L., Pitcher, J. A., et al. (1997) *J. Biol. Chem.* 272, 31051–31057.
39. ter Haar, E., Harrison, S. C., and Kirchhausen, T. (2000) *Proc. Natl. Acad. Sci. U.S.A.* 97, 1096–1100.
40. Kraulis, P. (1991) *J. Appl. Crystallogr.* 24, 946–950.
41. Guex, N., and Peitsch, M. C. (1997) *Electrophoresis* 18, 2714–2723.
42. Nicholls, A., Sharp, K., and Honig, B. (1991) *Proteins* 11, 281–296.

BI015905J